J. Fluid Mech. (1983), *vol.* 126, *pp.* 287–305
Printed in Great Britain

An experimental and theoretical investigation of the onset of convection in rotating spherical shells

By C. R. CARRIGAN† AND F. H. BUSSE

Department of Earth and Space Sciences, Institute of Geophysics and Planetary Physics, University of California, Los Angeles, CA 90024

(Received 24 July 1980 and in revised form 4 June 1982)

Convection in a rapidly rotating spherical layer with constant-temperature boundary conditions is studied in a laboratory experiment. The asymptotic theory of Busse (1970) is extended to permit a comparison with the observations of the onset of convection and its properties. It is found that the prediction of the power-law dependences of the critical buoyancy number and the critical wavenumber on the rotation rate are borne out, although discrepancies in the actual values of these quantities do exist. Calculations on the basis of equations proposed by Roberts (1968) show that a thermal wind that is present in the basic state of the model has a stabilizing influence on the onset of convection. Stewartson layers not taken into account in the asymptotic analysis for vanishing Ekman number E appear to be responsible for the remaining disagreement between theoretical predictions and observations at finite values of E.

1. Introduction

An understanding of buoyancy-driven flows in rotating systems is a prerequisite for elucidating many geophysical and astrophysical processes. In particular, the significance of these flows for heat and momentum transport and magnetic-field generation in planets and stars provides ample motivation to consider the fundamental problem of how rotation, through the Coriolis force, influences the stability of the basic state and the form of thermal convection in a spherical layer of fluid. The laboratory modelling of flows in rapidly rotating planets and stars is possible because motion is driven primarily by the component of body force perpendicular to the axis of rotation. This component of gravity in a planet or star has approximately the same radial dependence as the centrifugal body force used in the laboratory model. The fact that the direction of the centrifugal force in the model is roughly opposite to that of gravity is compensated for by a reversal of the temperature gradient since the motions depend only on the inner product between gravity and temperature gradient. There thus exists a dynamical analogy between buoyancy-driven flows in a laboratory model and those occurring in rotating stars and planets (Busse & Carrigan 1976). For a discussion of numerical solutions for convection in spherical shells and applications to the Sun we refer to Gilman (1976).

Convection instability can occur in fluids with a positive coefficient of thermal expansion when the scalar product of the temperature gradient and the body force is positive. The Rayleigh–Bénard instability in a non-rotating horizontal layer provides the simplest example of this mechanism. Motions set in when the buoyancy

† Permanent address: Sandia National Laboratories, Geophysics Research Division (5541), Albuquerque, NM 87185.

forces become sufficiently strong to overcome losses due to viscous dissipation and thermal diffusion, but in a rotating system the Coriolis force can vastly extend the range of stability of the basic state. The Coriolis constraint is best expressed by the Proudman–Taylor theorem for incompressible, inviscid and time-independent flows. In the absence of viscous and inertial forces, only the pressure gradient can balance the Coriolis force, i.e. geostrophic balance exists. Under these ideal conditions the theorem requires that flows be two-dimensional. Convection in a rapidly rotating cylindrical annulus with a cooled inner wall, a heated outer wall, and insulating and stress-free parallel endwalls is an example. The equations of motion permit solutions in the form of rolls aligned parallel to the rotation axis for which the Coriolis force exactly balances the pressure gradient. The problem thus becomes equivalent to the Rayleigh–Bénard case with rotation entering only through the centrifugal term, which replaces gravity $\mathbf{g}$ as the body force. In fact $\mathbf{g}$ can be neglected in the laboratory experiments when the rotation axis is vertical. Since the component of motion in the direction of gravity is vanishing, only the component of the body force perpendicular to the rotation axis is important for driving the flow.

In a cylindrical annulus with oppositely sloping top and bottom boundaries or in a sphere, flow with a radial component cannot follow geostrophic contours. Thus convection must deviate from geostrophic balance. This can be achieved for a strongly time-dependent inertial mode or for a weakly time-dependent mode with enhanced vorticity diffusion, the preferred mode of instability (Busse 1970). Vorticity diffusion is increased for the convection rolls with large azimuthal wavenumbers, which allows the weakening of adverse vorticity gradients caused by the non-geostrophic component of the flow. In this respect, viscosity is destabilizing even though viscous dissipation is increased. Also, the azimuthal scale of convection is not characterized by the depth of the layer as in the Rayleigh–Bénard case. According to linear theory, the azimuthal scale depends on the local inclination of the boundaries as well as on the Ekman and Prandtl numbers.

The linear problem for non-axisymmetric convection in a rapidly rotating sphere was initially considered in detail by Roberts (1968), who obtained normal-mode solutions for the perturbation equations. However, he assumed that the most-unstable mode had an axial velocity component that was symmetric about the equatorial plane. Investigating the problem initially in a cylindrical layer with inclined end boundaries and then extending to the spherical case, Busse (1970) found that the columnar mode corresponding to an antisymmetric axial component describes the realized form of convection in a rotating sphere (figure 1). Using the assumption that the radial scale of convection is large compared with the azimuthal scale, Roberts and Busse neglected the radial dependence in their asymptotic analyses.

Recently, Soward (1977) has investigated the spherical case in more detail and has obtained a solution to the nonlinear equations for the onset of convection in an internally heated sphere. He found that the critical value of the buoyancy parameter B obtained by Busse evidently underestimated the neutral stability by an amount given by

$$\frac{\Delta B}{B} \propto E^{\frac{2}{3}},$$

where E is the Ekman number. This represents a relatively small correction, typically 5 % under laboratory conditions, to the result of the linear theory. Soward's analysis implies, however, that the onset of convection in a rotating sphere is a finite-amplitude phenomenon; a modification of the basic-state temperature field evidently being necessary before a growing solution can exist. Any application of Soward's theory

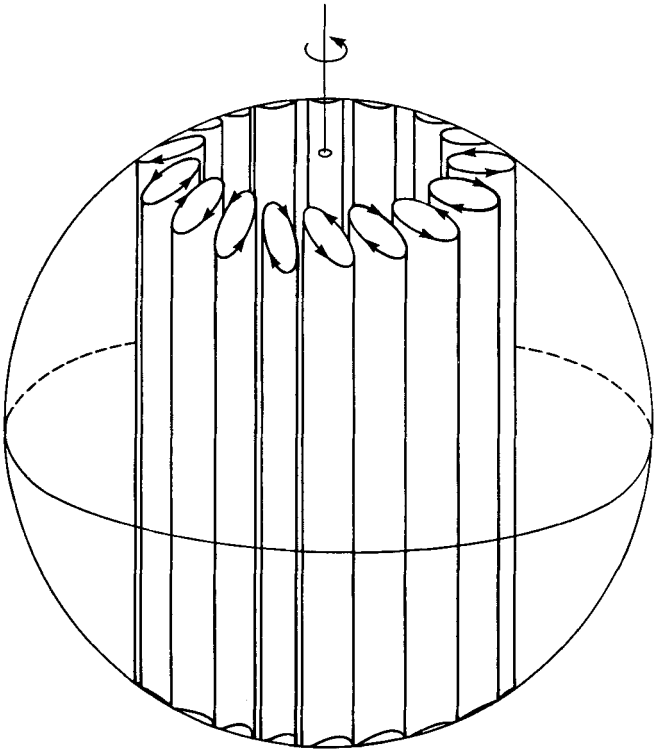

FIGURE 1. A sketch of the non-axisymmetric solution obtained by Busse (1970) for convection in a rapidly rotating and self-gravitating fluid sphere.

to the present experiment is at best qualitative, since the special conditions assumed by the theory do not correspond to those realized in the laboratory experiment.

Earlier laboratory experiments were performed by Busse & Carrigan (1974, hereafter referred to as I) to study the stability of the basic state in a rapidly rotating cylindrical layer formed by two concentric cylinders with different radii. The primary body force was centrifugal, and a destabilizing temperature gradient was produced across the layer by maintaining the outer cylinder at a higher temperature than the inner one. The local inclination of the spherical boundary was modelled by placing conical boundaries at the top and bottom of the cylindrical gap. Even though the inclinations were large compared with those assumed by the asymptotic theory, relatively good agreement between theory and observation was found.

The purpose of the present experiment is to investigate the properties of convection near onset in a spherical layer. An adaptation of the asymptotic theory for convection in a cylindrical annulus is derived for a comparison with measurements. Unlike the theoretical models originally considered by Roberts and by Busse, which assume a static initial state, a thermal wind is present in the basic state of the laboratory model owing to the deviation of the centrifugal potential surfaces from the spherical isotherms. A modification of Roberts' approach will be used to evaluate the stabilization of the basic state resulting from this shear flow. While complicating the analysis, the existence of a baroclinic basic state in the experiment is of interest by itself since it represents a common feature of stellar atmospheres and planetary cores. Although the theoretical analysis was motivated by the experiment, it is presented here first to provide a reference for the discussion of the observations.

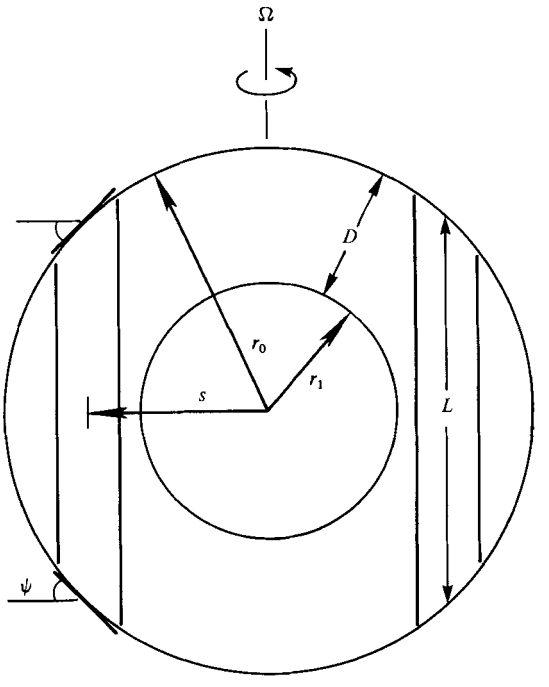

FIGURE 2. Cross-section of the spherical-layer geometry showing the relation to the narrow-cylindrical-gap geometry for which the onset of convection was investigated by Busse (1970). The cylindrically radial position of the gap determines both the inclination of the end boundaries as well as the height L of the gap.

2. Theoretical analysis

We consider the spherical fluid layer of thickness D bounded by two concentric spherical surfaces with radii r_1 and r_0, $r_1 \leqslant r_0$, as shown in figure 2. The outer and the inner spheres are kept at the temperatures T_0 and T_1 respectively, with T_0 exceeding T_1. The spherically symmetric solution for the temperature distribution is given by

$$T_s = \frac{T_0 r_0 (r - r_1) + T_1 r_1 (r_0 - r)}{r(r_0 - r_1)}. \tag{1}$$

When the gravity distribution is spherically symmetric, the basic equations admit the static solution. But in the laboratory system the spherical shell rotates about a vertical axis and the centrifugal force is not everywhere parallel to the density gradient. The resulting baroclinicity of the basic state induces an axisymmetric azimuthal flow, called the 'thermal wind' in the meteorological context. By assuming the density dependence

$$\rho = \rho_0[1 - \gamma(T - T_0)] \tag{2}$$

and taking the curl of the equation of motion with respect to the system rotating with angular velocity $\boldsymbol{\Omega}\mathbf{k}$, where $\mathbf{k}$ is the vertical unit vector, we obtain

$$\begin{aligned} -2\boldsymbol{\Omega}\mathbf{k} \cdot \nabla \hat{\mathbf{U}} &= \frac{-\gamma(T_0 - T_1)}{r_0 - r_1} \nabla \frac{r_1 r_0}{r} \times [\Omega^2 \mathbf{k} \times (\mathbf{r} \times \mathbf{k})] \\ &= \frac{-\gamma(T_0 - T_1)}{r_0 - r_1} \Omega^2 \frac{\mathbf{k} \cdot \mathbf{r}\, r_1 r_0}{r^3} \mathbf{k} \times \mathbf{r}. \end{aligned} \tag{3}$$

Integration yields the solution for the thermal wind $\hat{\mathbf{U}}$:

$$\hat{\mathbf{U}} = -\gamma \frac{(T_0 - T_1)}{r_0 - r_1} \frac{r_1(r_0 - r)}{2r} \Omega \mathbf{k} \times \mathbf{r}, \tag{4}$$

where the constant of integration has been chosen such that $\hat{\mathbf{U}}$ vanishes at the outer boundary. Since viscous forces have not been taken into account in (3), the no-slip condition at the inner spherical boundary cannot be satisfied. This will change the solution (4) inside the cylindrical surface touching the inner sphere at the equator, but, in the limit of high rotation rates Ω, it will not change the solution outside the cylindrical surface where all boundary conditions are satisfied. In the laboratory realization of the system, ordinary gravity induces a thermal wind similar to that given by (4). But, since the centrifugal force far exceeds gravity in typical cases, the gravity-induced azimuthal flow has not been included in (4).

The basic state described by (1) and (4) becomes unstable to non-axisymmetric disturbances when the centrifugal force becomes sufficiently strong. In order to derive the conditions for instability we use dimensionless variables based on the gap thickness $D \equiv r_0 - r_1$, Ω^{-1} and $T_0 - T_1$ as scales for length, time and temperature respectively. The linearized equations for the disturbance velocity field $\mathbf{v}$ and the deviation θ from the basic temperature field (1) are given by

$$\left(\frac{\partial}{\partial t} + \mathbf{U} \cdot \nabla\right) \mathbf{v} + \mathbf{v} \cdot \nabla \mathbf{U} + 2\mathbf{k} \times \mathbf{v} = -\nabla \pi - \mathbf{i} B \theta s R^{-1} + E \nabla^2 \mathbf{v}, \tag{5a}$$

$$\nabla \cdot \mathbf{v} = 0, \tag{5b}$$

$$\left(\frac{\partial}{\partial t} + \mathbf{U} \cdot \nabla\right) \theta = -\mathbf{v} \cdot (s\mathbf{i} + z\mathbf{k})\, R^2 \xi (s^2 + z^2)^{-\frac{3}{2}} + E P^{-1} \nabla^2 \theta. \tag{5c}$$

We have introduced a cylindrical system of coordinates (s, ϕ, z) with the z-coordinate in the direction of $\mathbf{k}$. The unit vector $\mathbf{i}$ is defined by $\mathbf{i} = \nabla s$. The dimensionless azimuthal flow $\mathbf{U}$ is given by

$$\mathbf{U} = U \mathbf{k} \times \mathbf{i} s \equiv -\tfrac{1}{2} B \mathbf{k} \times \mathbf{i} s \xi [R(s^2 + z^2)^{-\frac{1}{2}} - 1], \tag{6}$$

where ξ denotes the radius ratio r_0/r_1, and $R \equiv (1 - \xi)^{-1}$ is the dimensionless radius of the spherical shell. The physical parameters enter the problem in the form of three dimensionless parameters:

$$\begin{aligned} \text{buoyancy number} \quad & B \equiv \gamma (T_0 - T_1)\, r_0 / D, \\ \text{Ekman number} \quad & E \equiv \nu / \Omega D^2, \\ \text{Prandtl number} \quad & P \equiv \nu / \kappa, \end{aligned}$$

where ν is the kinematic viscosity and κ is the thermal diffusivity of the fluid. The effects of ordinary gravity have been neglected in (5). As in the case of (3), the Boussinesq approximation has been used in (5), implying that the temperature dependence is taken into account only in connection with the centrifugal-force term. All terms that can be written as a gradient are included in $\nabla \pi$. In contrast with (3), the viscous force has been included, even though the limit of small E is of primary interest. As the results of the analysis demonstrate, the scale of the convective motions decreases with E in contrast with the order-unity scale of the flow (6).

The primary boundary condition to be satisfied by the solution of (5) is

$$\mathbf{v} \cdot (s\mathbf{i} + z\mathbf{k}) = 0 \quad \text{at} \quad z = \pm (R^2 - s^2)^{\frac{1}{2}}. \tag{7}$$

Other boundary conditions are of secondary importance and may be satisfied by the

addition of Ekman layers or Stewartson layers to the solutions derived below. This will not affect the conditions for the onset of instability in the limit $E \to 0$.

The analysis of (5) is based on the assumption that the solution is vanishing except in the neighbourhood of the cylindrical surface $s = s_0$, with $\xi R < s_0 < R$. Two approaches towards an approximate solution will be used. Explicit expressions are obtainable by following the approach of Busse (1970), while a more accurate description can be obtained by following Roberts' (1968) analysis of a related problem and solving numerically an ordinary differential equation. Since the problem does not depend on t and ϕ explicitly, an exponential dependence on these variables can be presumed for θ and $\mathbf{v}$. In the first approach it is assumed the velocity field is approximately geostrophic,

$$\mathbf{v}_0 = -\tfrac{1}{2}\nabla \times \mathbf{k}\pi_0 \equiv -\tfrac{1}{2}\nabla \times \mathbf{k}p(s) \exp(i\omega t + im\phi). \tag{8}$$

After taking the $\mathbf{k}$-component of the curl of (5a), averaging it over the interval $-(R^2-s_0^2)^{\frac{1}{2}} \leqslant z \leqslant (R^2-s_0^2)^{\frac{1}{2}}$, applying the boundary condition (7) in order to eliminate $\mathbf{k}\cdot\mathbf{v}$ at the boundaries, and replacing $\mathbf{v}$ everywhere else by (8), the following equation for $p(s)$ is obtained:

$$\left\{\left[i\omega + i\bar{U}m - E\left(\frac{\partial^2}{\partial s^2} - a^2\right)\right]\left(\frac{\partial^2}{\partial s^2} - a^2\right) - \frac{2im}{R_2 - s_0^2}\right\}\pi_0 = -\frac{2Bim\bar{\theta}}{R}, \tag{9}$$

where $a = m/s_0$, and the overbar indicates the average over the z-interval. In order to eliminate the averaged temperature disturbance $\bar{\theta}$, (8) is used in place of $\mathbf{v}$, and, for simplicity, U and the static temperature gradient are replaced by their averaged values

$$\bar{U} \approx -B\xi\frac{R}{2s_0}\overline{(1-z^2(R^2-s_0^2))} = -\frac{B\xi R}{3s_0}, \quad \overline{R^2(s_0^2+z^2)^{-\frac{3}{2}}} = Rs_0^{-2}. \tag{10}$$

This latter procedure is not really necessary, but allows us to obtain explicit expressions for B and ω. We anticipate that the ϕ-dependence predominates over the s-dependence of π_0, and we therefore neglect the latter. Thus (9) can be replaced by the complex algebraic equation for the two unknowns ω and B

$$[(i\omega + im\bar{U} + Ea^2)\,a^2 + 2im(R^2-s_0^2)^{-1}]\,(i\omega + im\bar{U} + P^{-1}Ea^2) = a^2B\xi. \tag{11}$$

The imaginary and real parts of this equation yield

$$\omega = -m\bar{U} - \frac{2m}{(1+P)\,a^2(R^2-s_0^2)}, \tag{12}$$

$$B\xi = P^{-1}E^2a^4 + \frac{4Ps_0^2}{(R^2-s_0^2)^2\,a^2(1+P)^2} \tag{13}$$

respectively. The minimum value of B as a function of a and s_0 in the interval $\xi < s_0/R < 1$ is reached as s_0 approaches ξR:

$$B_c = 3\xi^{-1}P^{-1}\left(\tfrac{1}{2}E\left[\frac{P2\xi}{(1+P)\,R(1-\xi^2)}\right]^2\right)^{\frac{2}{3}}. \tag{14}$$

The corresponding value of the wavenumber is given by

$$a_c = \left(\frac{\sqrt{2}\,\xi P}{(1+P)\,R(1-\xi^2)\,E}\right)^{\frac{1}{3}}. \tag{15}$$

In the above analysis, the critical value B_c is not affected by the presence of the thermal wind shear in the basic state because of the various approximations that have

been made. But it is likely that it has a stabilizing effect. To take into account this effect and in order to represent more accurately the deviations from the geostrophic state caused by the finite inclination of the boundaries, we follow Roberts' (1968) asymptotic method in the limit $E \to 0$. Using his representation for the solenoidal velocity field $\mathbf{v}$,

$$\mathbf{v} = \nabla \times [\nabla \times \mathbf{k} J(as)\, \Phi(z) \exp(im\phi + i\omega t)] + \nabla \times \mathbf{k} J(as)\, \Psi(z) \exp(im\phi + i\omega t),$$

in (5), then eliminating θ, π, and Φ from the resulting equations, and finally introducing new variables

$$\zeta = \frac{a}{R}, \quad \tilde{a} = a(\tfrac{1}{2}ER)^{\frac{1}{3}}, \quad \tilde{\omega} = \omega\left(\frac{R^2}{4E}\right)^{\frac{1}{3}}, \quad \tilde{B} = B\left(\frac{R^2}{4E}\right)^{\frac{2}{3}},$$

one obtains the following equation for $\Psi(z)$:

$$\left(\frac{d}{d\zeta} - \frac{\tilde{B}\xi^2\zeta i\tilde{a}}{(\xi^2+\zeta^2)^{\frac{3}{2}}(P^{-1}\tilde{a}^2 + i\tilde{a}f + i\tilde{\omega})}\right)\frac{d\Psi/d\zeta}{(\tilde{a}^2 + i\tilde{a}f + i\tilde{\omega})\,\tilde{a}^2}$$
$$= \left(\tilde{a}^2 + i\tilde{a}f + i\tilde{\omega} - \frac{\tilde{B}\xi^3(\xi^2+\zeta^2)^{-\frac{3}{2}}}{\tilde{a}^2P^{-1} + i\tilde{a}f + i\tilde{\omega}}\right)\Psi, \quad (16)$$

where the function f is defined by

$$f(\zeta) = -\tilde{B}\xi^2[(\xi^2+\zeta^2)^{-\frac{1}{2}} - 1]. \quad (17)$$

Equation (16) is equivalent to (5.2) of Busse (1970) except that the thermal wind (6) and the different static temperature distribution (1) have been taken into account. Equation (16) has been solved numerically using a Runge–Kutta method. The parameters $\tilde{B}$ and $\tilde{\omega}$ are determined as functions of $\tilde{a}$ by applying the boundary condition

$$\zeta\frac{d}{d\zeta}\Psi + i(\tilde{a}^2 + i\tilde{a}f + i\tilde{\omega})\,\tilde{a}\xi\Psi = 0 \quad \text{at} \quad \zeta = \pm(1-\xi^2)^{\frac{1}{2}}. \quad (18)$$

Since the lowest value of $\tilde{B}$ corresponds to an even function $\Psi(\zeta)$, the integration can be started with $\partial\Psi/\partial\zeta = 0$ at $\zeta = 0$. Real and imaginary parts of (18) then yield two expressions that vanish only for certain values of $\tilde{B}$ and $\tilde{\omega}$. By iterating with a Newton–Raphson method, these values can be determined. The minimum value of $\tilde{B}$ as a function of $\tilde{a}$ represents the critical value for the onset of convection. The results resemble closely the approximate relationships (14) and (15) for B_c and a_c except for an increase of B_c due to the stabilizing influence of the thermal wind (4).

Unfortunately, the asymptotic solutions obtained from (16) are not likely to agree well with experimental data at finite rotation rates. Because the thermal-wind solution (4) is valid only outside the cylindrical surface touching the inner sphere at the equator, a discontinuity at this surface must be expected. This discontinuity of the inviscid solution gives rise to a Stewartson layer with a radial thickness of order $E^{\frac{1}{4}}$, which adds a strong shear in the direction of the s-coordinate to the shear in the z-direction that has been taken into account in (19). But the s-dependence of the convection columns is not considered explicitly in the problem because of the assumption (18). A much more complex problem must therefore be considered at finite values of E in order to model faithfully the effect of radial shear close to the cylindrical surface where the onset of convection occurs.

According to Soward (1977), the extent of convection in the s-direction is of order $E^{\frac{1}{3}}$. Since this is large compared with the thickness of the order of $E^{\frac{1}{4}}$ of the Stewartson layers, the onset of convection should not be affected by the radial shear in the asymptotic limit $E \to 0$ on which the derivation of (19) has been based. But since

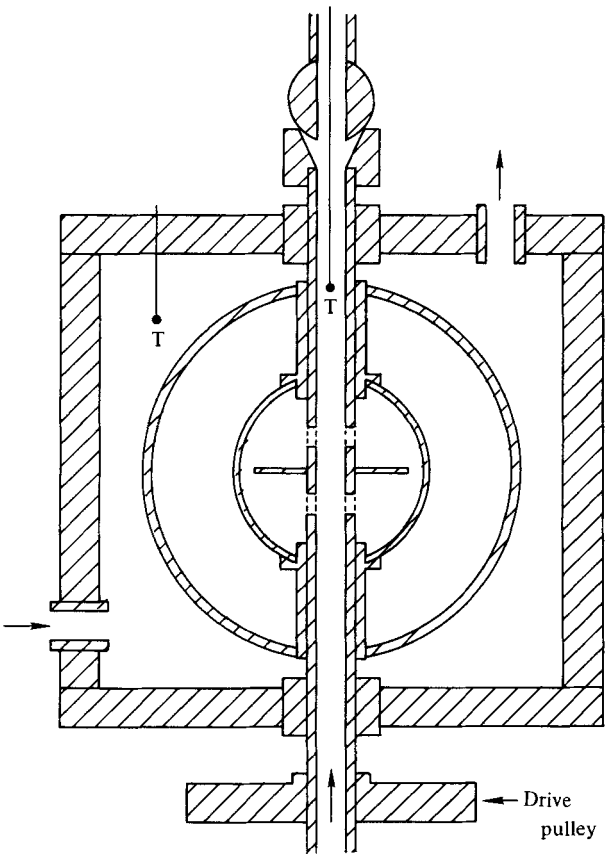

FIGURE 3. Cross-section of spherical-convection experiment consisting of two spheres mounted concentrically on a rotation shaft and contained in a Plexiglas box which acts as a waterjacket. Thermocouples are denoted by T.

sufficiently high rotation rates are not accessible in the present experiment only a tendency towards quantitative agreement between theory and observations can be expected.

3. Experimental apparatus and technique

Figure 3 is a cross-sectional view of the experimental apparatus. A transparent Plexiglas box acting as a water jacket surrounds two spheres, which are mounted concentrically on a rotation shaft. The layer or gap formed by the spheres is filled with a working fluid, which is either water or ethylene glycol. The outer sphere, with an inner diameter of 100 mm, is made of Plexiglas so that visual observations of flows in the gap can be made. An aluminium or stainless-steel inner sphere is used. The gap width can be changed by using inner spheres of different diameters. Extending through the top and bottom of the box via waterproofed bearing mounts that support it, the rotation shaft is driven by a variable-speed motor capable of maintaining rotation rates of up to 1000 r.p.m. to within 1 % over long periods. A temperature difference accurate to within 0·02 °C is maintained across the spherical gap by circulating warm water through the box to heat the outer sphere and cooler water

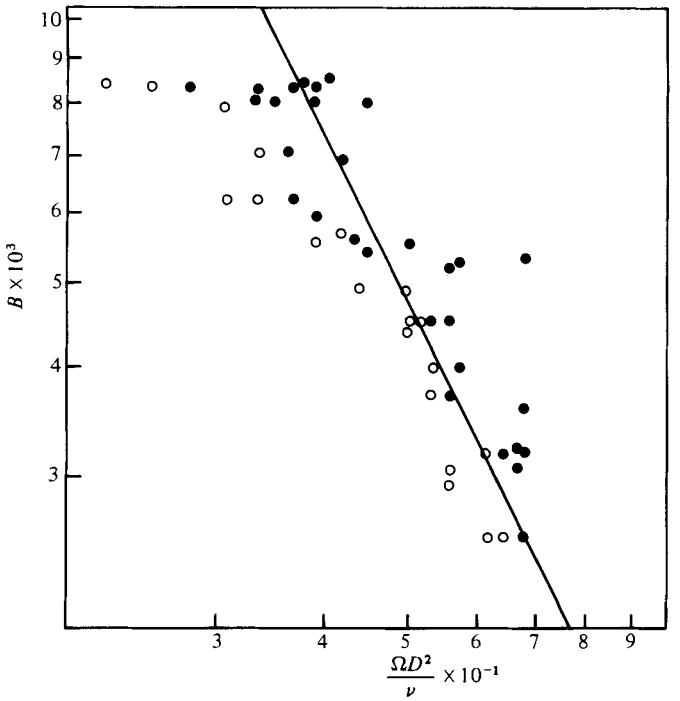

FIGURE 4. Onset of convection when interior dissipation dominates. Ethylene glycol ($\nu = 0{\cdot}14$ St, $P = 145$) was used in a layer with $D = 3{\cdot}00 \pm 0{\cdot}20$ mm, where $r_1 = 44{\cdot}65$ mm and $r_0 = 47{\cdot}65$ mm, a constant for all experiments. In this and following neutral-stability diagrams, filled circles indicate observation of convection columns; open circles indicate that convection was not observed.

through the inner sphere via the hollow rotation shaft, which is connected to the coolant circuit using ball-and-socket couplings. The mean temperature for most of the experiments is 28 °C, although one set of observations is obtained using water with a mean temperature of 46 °C to investigate the effect of lowering the Prandtl number from 5·7 to 3·85. The onset of convection in the gap is always determined visually using microscopic neutrally buoyant platelets that align along the shear and reflect light inhomogeneously, allowing the convection columns to be photographed with the aid of a stroboscopic light source. The timescale for the evolution of the basic state is of the order of 300 s for the largest gap used, so that observation periods of thirty minutes were found to be sufficient for establishing the basic state and the onset of convection for supercritical temperature gradients. For further details on the experimental technique, the reader is referred to I.

4. Results and analysis

Ethylene glycol ($\nu = 0{\cdot}14$ St, $P = 145$) is used as the working fluid in the small-gap (3·00 mm) geometry to investigate the limit of dominating interior dissipation. Strong viscous diffusion has the effect of almost completely releasing rotational constraints so that the onset of thermal motions is determined mainly by viscosity and thermal diffusivity, although rotation exerts an orientational effect since the rolls are aligned with the rotation axis. The application of the Rayleigh–Bénard criterion is appropriate

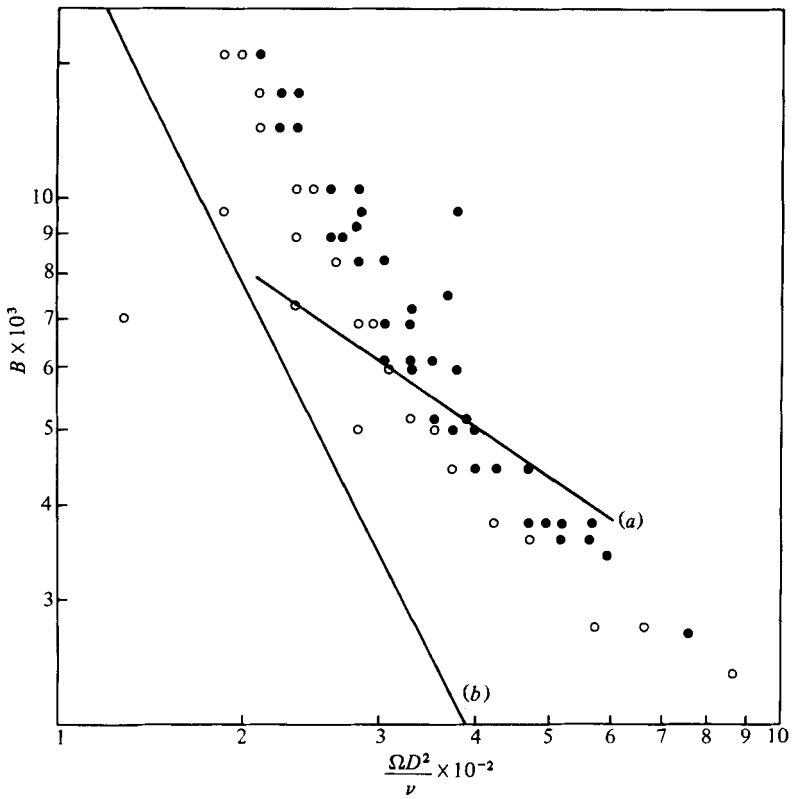

FIGURE 5. Onset of convection for a spherical layer of water with $D = 3{\cdot}00 \pm 0{\cdot}20$ mm. The lines (*a*) and (*b*) represent the asymptotic and Rayleigh–Bénard stability criteria respectively.

in the limit of Ekman numbers of the order 10^{-1} or larger. Using the buoyancy parameter, the criterion for the onset of convection is

$$B \geqslant B_c = 1708 \frac{E^2}{P}. \tag{19}$$

Since the curvature of the boundaries has a negligible effect in the small-gap limit, we have used the critical value (1708) of the Rayleigh number for plane parallel rigid boundaries. The dependence of B_c on E, and hence Ω, reveals the fact that the centrifugal force provides thermal buoyancy.

Figure 4 is a plot of observations of convection and its absence as a function of B and E^{-1}. The observations clearly define a boundary of neutral stability. For reference the neutral-stability line representing (19) has been included. For larger values of E^{-1} the data for onset are in excellent agreement with the Rayleigh–Bénard criterion and provide a good test for systematic errors of measurement of such quantities as thermal diffusivity, layer depth and temperature differences. The slope of the experimental line is in agreement with the rotation rate, entering the problem only in the buoyancy term (Ω^2). For the low-rotation end of the regime diagram, the Earth's gravity probably cannot be neglected and, because of strong viscous diffusion, rotational constraints are not sufficiently strong to prevent the release of potential energy in the form of baroclinic instability. The fact that a strong thermal wind has been observed at low rotation rates along with the qualitatively different appearance of the instability supports this conclusion.

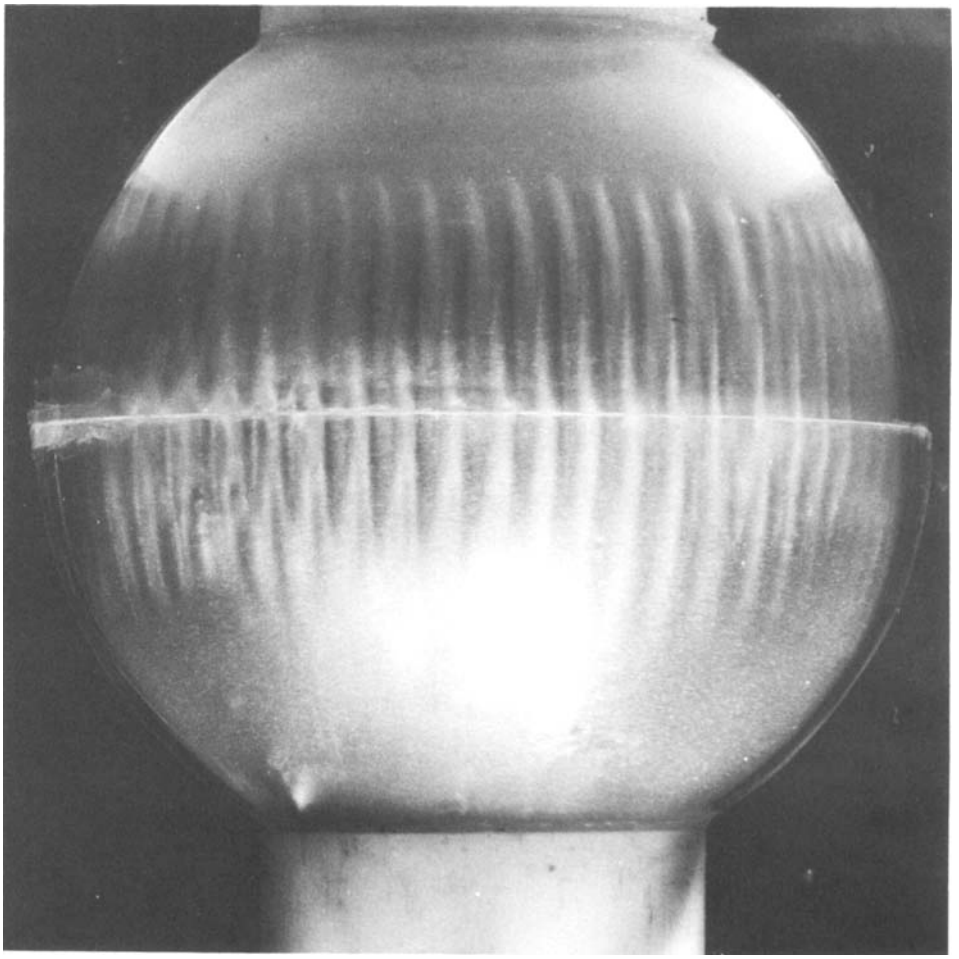

FIGURE 6. Columnar convection occurring in the narrow-gap (3·00 mm) geometry. The convecting fluid is water with a mean temperature of 28 °C ($\nu = 0{\cdot}01$ St, $P = 5{\cdot}7$). Tiny platelets in the fluid allow visualization of the columns.

Significantly different results were obtained when water at 28 °C ($\nu = 0{\cdot}01$ St, $P = 5{\cdot}7$) was used in the spherical gap. The empirical neutral-stability boundary in figure 5 is evident from the observations. The lowest line represents the Rayleigh–Bénard criterion and, as mentioned above, the neutral stability observed at lower rotation rates appears to have the same dependence on rotation that characterizes the Rayleigh–Bénard limit. For higher values of the rotation rate (E^{-1}), the empirical results exhibit a weaker dependence than Ω^2 as the stabilizing effects of inclined boundaries become more important. The new slope is more characteristic of the line labelled (*b*), which was obtained from (14). While this criterion has been included for comparison, it is really more appropriate for the larger-gap experiments since the convection columns are assumed to end on inclined boundaries, which they do not do for the small-gap experiments. In figure 6 it can be seen that the columns are deformed by the steep outer spherical boundary, which acts more as a sidewall than an inclined top or bottom in the sense of the cylindrical geometry.

Figure 7 indicates the empirical dependence of the azimuthal wavenumber on rotation. Rayleigh–Bénard theory would predict $\alpha_{RB} = 3{\cdot}117$, but at the low-rotation

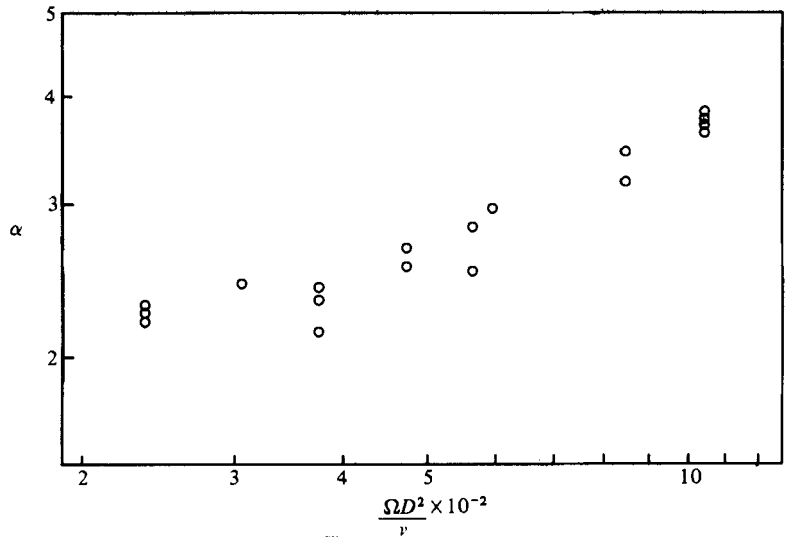

FIGURE 7. Observations of the azimuthal wavenumber α, as a function of E^{-1} for the small-gap water case. Rayleigh–Bénard theory predicts $\alpha_{RB} = 3{\cdot}117$.

end, where the empirical neutral stability possesses a dependence on the rotation rate similar to the predictions of Rayleigh–Bénard theory, it is observed that the wavenumber is significantly less than α_{RB}. This may be interpreted as an effect of the Plexiglas outer boundary, the thermal conductivity of which is actually lower than that of the contained fluid. For boundaries of finite thermal conductivity Sparrow, Goldstein & Jonsson (1964) have shown that temperature perturbations need not vanish at the boundaries as is necessary for the infinitely conducting case, with the result that the thermal scale is larger than the layer depth. With this increase in thermal scale, they found an attendant increase in the scale of the convective motions. In the high-rotation rate region of figure 7, the azimuthal wavenumber is observed to exceed the Rayleigh–Bénard prediction; a result that can be readily explained in terms of the increased importance of rotational constraints and the necessity for enhanced vorticity diffusion that results from a decrease in the azimuthal scale.

The other two experiments carried out with water were of the wide-gap geometry ($D = 9{\cdot}55$ mm, $22{\cdot}25$ mm). Comparison of the views of the meridional plane in figure 8(a) with the equatorial plane in figure 9 shows the striking differences in scale between the azimuthal and radial flows in these experiments. Such observations are consistent with the linear theory's prediction of an azimuthal wavenumber that is large compared to the radial wavenumber, a condition that follows from the minimization of the buoyancy parameter. The observations of both the buoyancy parameter and the wavenumber at onset for the two gaps with $P = 5{\cdot}7$ are presented in figures 10(a, b) and 11, and the observations in the case $D = 22{\cdot}25$ mm, $P = 3{\cdot}85$ are given in figure 10(c).

The observed neutral-stability curve is underestimated by (14) (solid lines) by about 10–25 % in the $D = 9{\cdot}55$ mm, $P = 5{\cdot}7$ experiment, and by nearly 50 % in the $D = 22{\cdot}25$ mm, $P = 5{\cdot}7$ case. However, the agreement improved somewhat in this latter experiment if the Prandtl number is reduced (figure 11a). The observed wavenumbers in the $P = 5{\cdot}7$ cases are only half as large as predicted by (15). But

the asymptotic theory does predict correctly the power-law dependences of B_c and a_c on the rotation rate.

The calculations based on (16) for the critical values B_c of the buoyancy parameter and the critical wavenumber are shown in the figures by the dashed lines. Although the inclusion of the stabilizing effect of the shear of the thermal wind in the z-direction reduces the discrepancy between theory and observation in some cases, the vertical shear does not appear to be the major source of the discrepancy. The strong radial shear at the rigid equatorial boundary of the inner sphere appears to be the main reason for the disagreement between theory and experiment in the range of Ekman number E investigated. It also seems reasonable that the radial shear favours the onset of convection columns with small azimuthal wavenumbers, which are less subject to the inhibiting influence of the shearing action. This could explain why the wavenumbers observed in the experiment are much smaller than predicted. A more-general theory, taking into account the radial shear, is desirable, but has not been attempted yet.

According to (12) and (15), the approximate asymptotic theory predicts a weak drift of the convection columns that is in the prograde or retrograde direction, depending on whether the upper or lower inequality in the relationship

$$\xi \lessgtr \frac{P+[4(1+P)^2+P^2]^{\frac{1}{2}}}{2(1+P)}$$

is satisfied. Since drift rate is of the order $E^{\frac{2}{3}}$ and because neither of the above inequalities is strongly satisfied in the various experiments, it is not surprising that no definite drift could be observed within the scatter of the data.

The dependence of the drift rate on the distance from the axis tends to wind the radially elongated modes into an increasingly tight spiral pattern. Such a prograde spiral pattern is indeed observed, as shown in the equatorial view of figure 9, but as a steady phenomenon. Viscous forces apparently limit the amount of spiralling. Soward (1977) has predicted that nonlinear effects lead to a stationary spiralling form of convection in special cases. But numerical computations by Cuong (1979) exhibit spiralling solutions of the linear equations.

5. Concluding remarks

The effect of rotation on thermal convection in a spherical fluid shell with a spherically symmetric gravity distribution may best be examined by separating the fluid region into two parts. Interior to a cylindrical surface, which touches the inner boundary at the equator, $\mathbf{g}$ and $\boldsymbol{\Omega}$ are nearly parallel, and a highly non-geostrophic three-dimensional form of convection is expected to exist (Busse & Cuong 1977). Exterior to this surface, the flow is mainly geostrophic, and only this region has been considered here. While general agreement between theory and observations has been found in all qualitative aspects of the study, a quantitative comparison is limited by complications associated with a centrifugally driven thermal-wind solution that characterizes the basic state. In the basic state a Stewartson layer exists in the region adjacent to the inner sphere where the onset of convection is also known to occur. The layer thickness varies as $E^{\frac{1}{4}}$, while the width of the convection zone varies as $E^{\frac{1}{3}}$. In the limit of vanishing E the zone will be unaffected by the presence of the layer, but sufficiently small values of the Ekman number cannot be realized in the experiment for this case to be approached. Convection produced in a sphere by

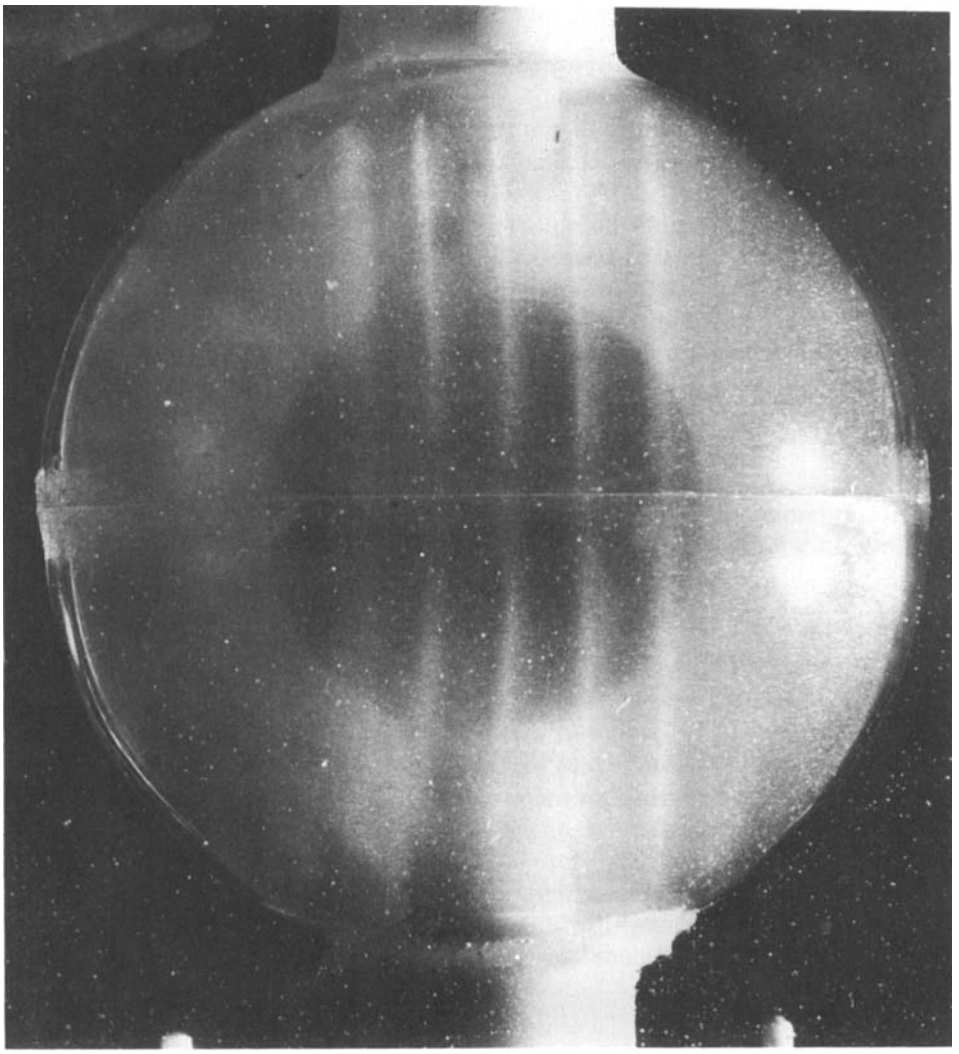

(a)

FIG. 8(a) For caption see facing page.

varying the boundary temperature linearly in time may provide a better test of the theories, since the inner sphere can be deleted, thereby eliminating the Stewartson layer. The observations of such an experiment will be presented in a future paper.

Very little information is available either from experimental observations or from theoretical computations about the state of high-amplitude convection in the limit of high rotation rates. The convection columns that are attached to the inner sphere when the buoyancy parameter is close to its critical value tend to fill the entire spherical shell outside the cylindrical surface, touching the inner sphere at the equator as the buoyancy parameter is increased. It is remarkable that the perfect alignment with the axis of rotation persists even at a high value of B. Because of different drift rates and wavelengths of columns at different distances from the axis, a non-uniform statistical pattern emerges, as shown in figure 8(*b*). No detailed measurements of this turbulent state of convection have been performed.

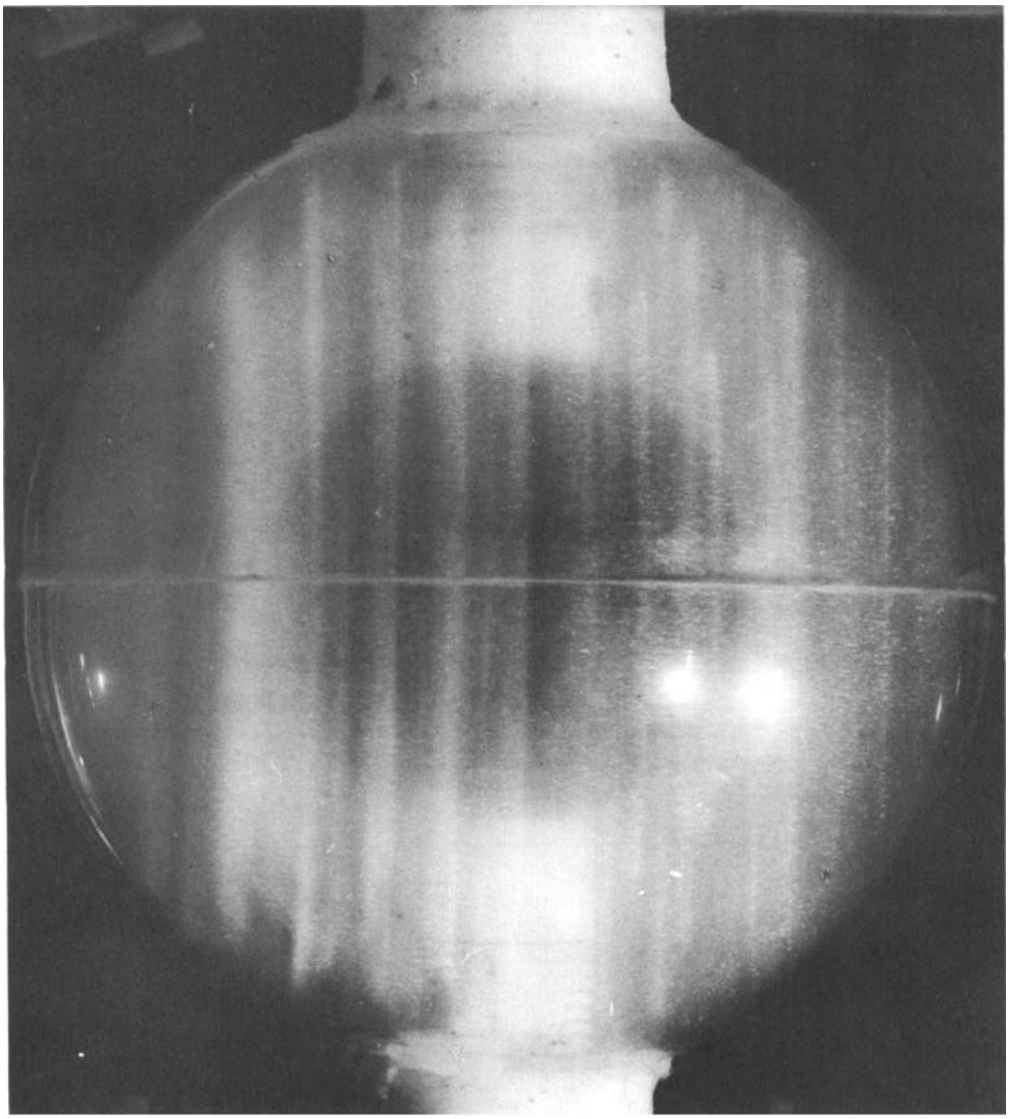

(*b*)

FIGURE 8. (*a*) The onset of convection in the wide spherical gap ($D = 22{\cdot}25$ mm) filled with water, the azimuthal wavelength of the columns is only a fraction of the gap width. (*b*) Same as in (*a*) but for a much larger Rayleigh number.

The research reported in this paper has been supported by the Geophysics Section of the U.S. National Science Foundation. The authors are indebted to Mr M. Nagata for his assistance in the computational part of the research. Juanene Gallaway skilfully typed the manuscript. The work at Sandia National Laboratories was supported by the U.S. Department of Energy under Contract no. DE-AC04-76DP00789.

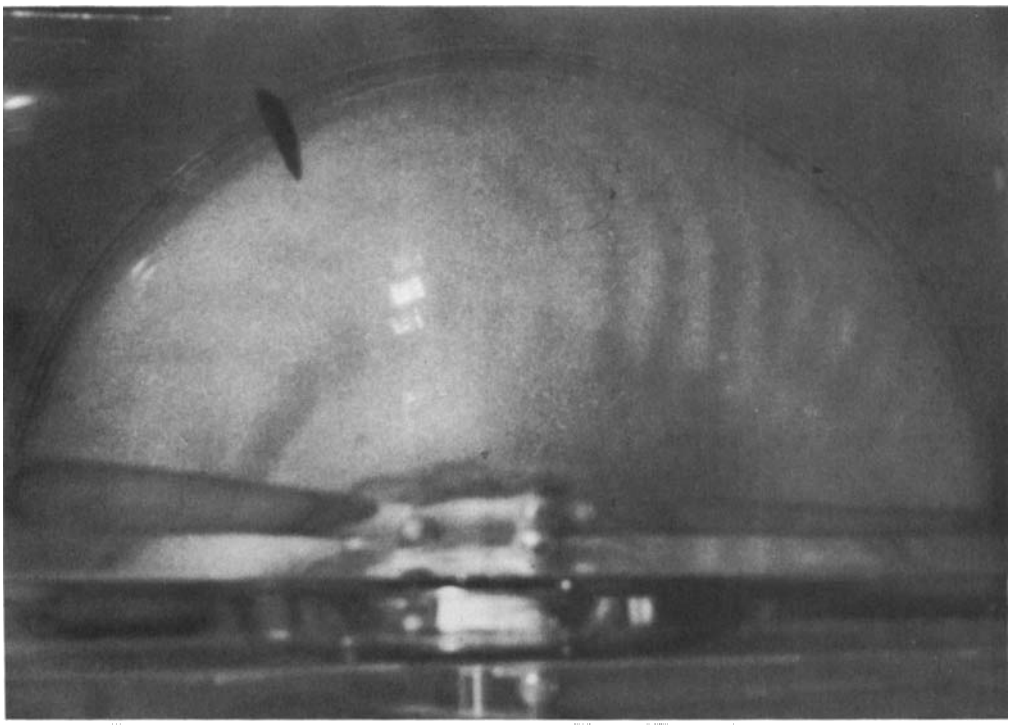

FIGURE 9. Equatorial view of convection near onset in the wide-gap geometry. The radial wavelength of the columns is approximately equal to the gap width. The spiralling of the cells is in the prograde direction.

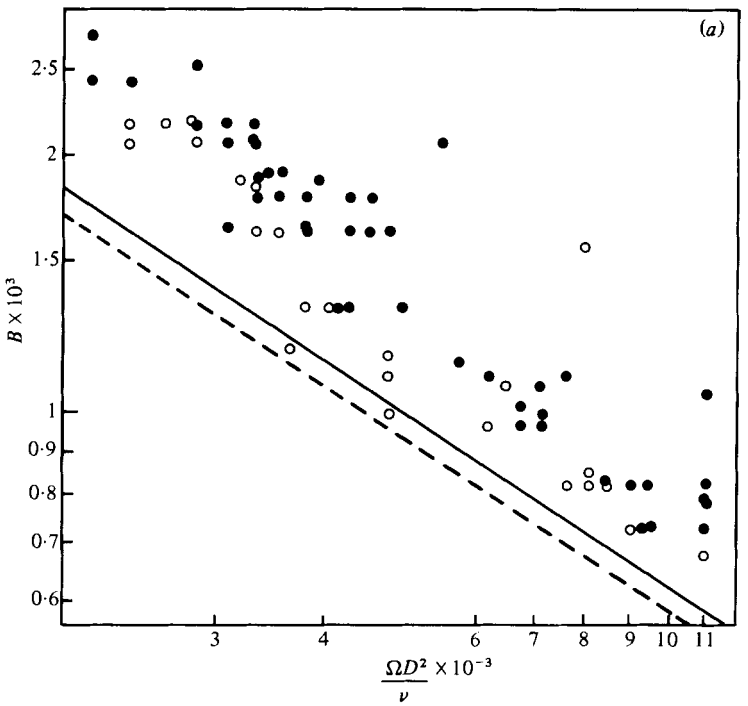

FIG. 10(a). For caption see facing page.

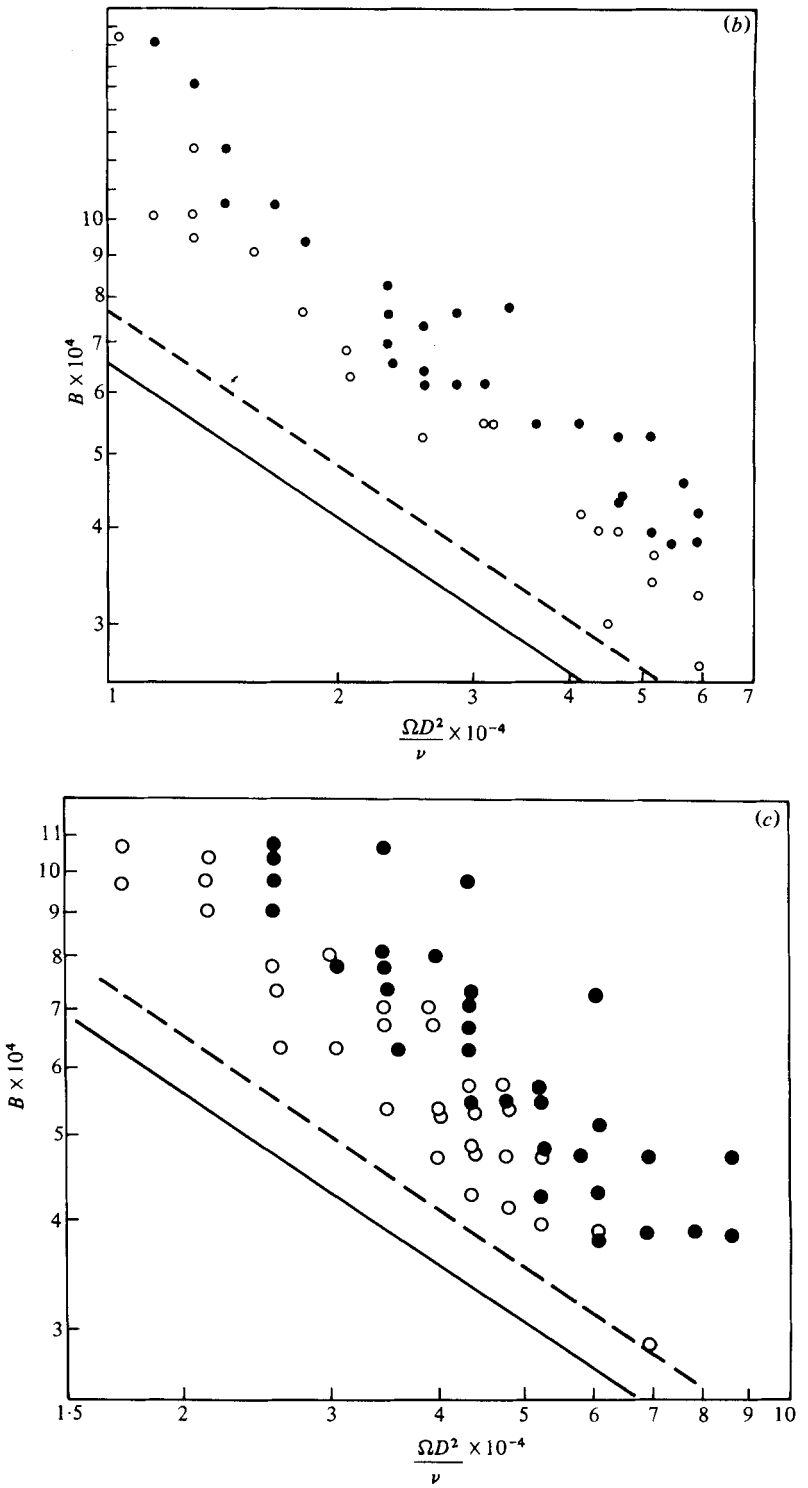

FIGURE 10. Observations of the convective instability in a spherical layer of water $P = 5{\cdot}7$. In this and the following figures, the predictions of the asymptotic theory and the numerical calculations which include the effects of the thermal wind are given by the solid and dashed lines respectively. (*a*) $D = 9{\cdot}55$ mm, $P = 5{\cdot}7$; (*b*) 22·25 mm, 5·7; (*c*) 22·25 mm, 3·85.

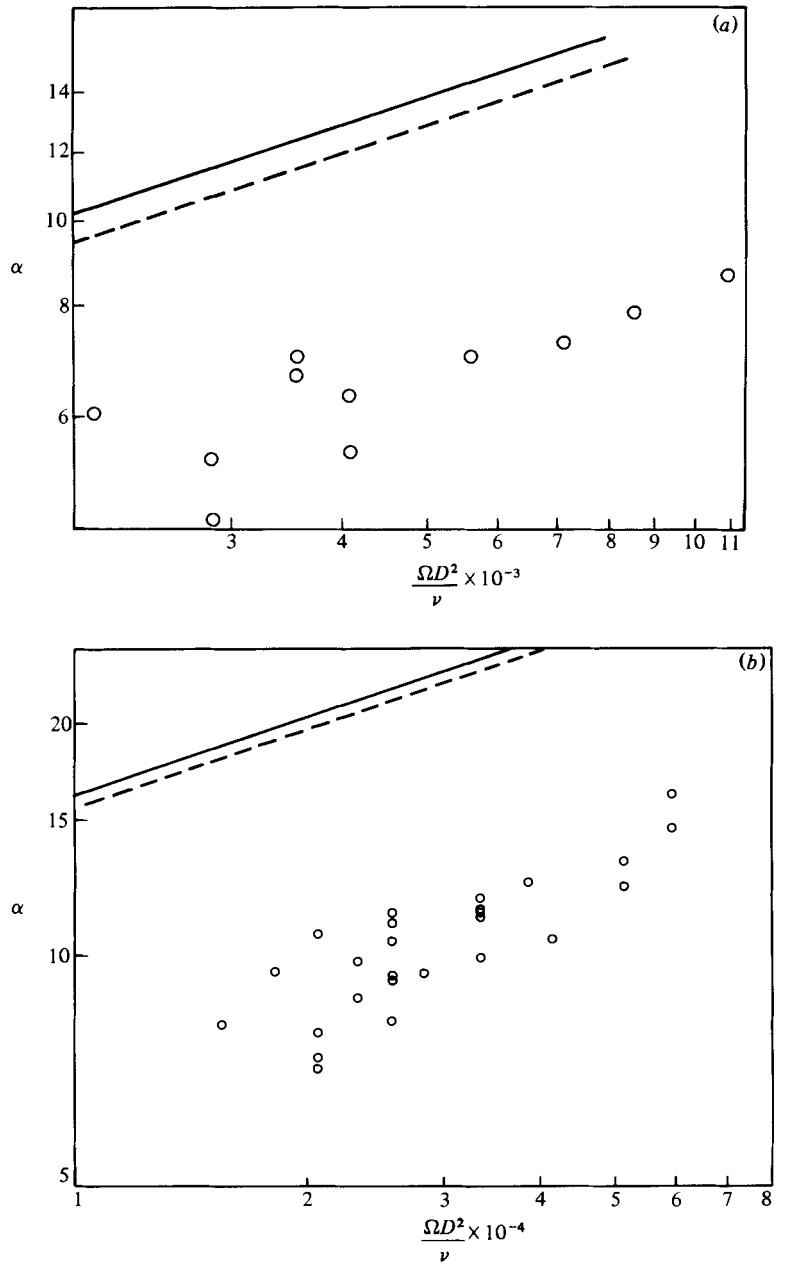

FIGURE 11. Observations of the azimuthal wavenumber α of convection for (*a*) the $D = 9{\cdot}55$ mm experiment and (*b*) the $D = 22{\cdot}25$ mm experiment, with $P = 5{\cdot}7$.

REFERENCES

BUSSE, F. H. 1970 Thermal instabilities in rapidly rotating systems. *J. Fluid Mech.* **44**, 441–460.

BUSSE, F. H. & CARRIGAN, C. R. 1974 Convection induced by centrifugal buoyancy. *J. Fluid Mech.* **62**, 579–592.

BUSSE, F. H. & CARRIGAN, C. R. 1976 Laboratory simulation of thermal convection in rotating planets and stars. *Science* **191**, 81–83.

BUSSE, F. H. & CUONG, P. G. 1977 Convection in rapidly rotating spherical fluid shells. *Geophys. Astrophys. Fluid Dyn.* **8**, 17–44.

CUONG, P. G. 1979 Thermal convection and magnetic field generation in rotating spherical shells. Ph.D. dissertation, University of California, Los Angeles.

GILMAN, P. A. 1976 Theory of convection in a deep rotating spherical shell and its application to the Sun. In *Proc. IAU Symp. no.* 71. *Basic Mechanisms of Solar Activity* (ed. V. Bumba & J. Kleczek), pp. 207–228. Reidel.

ROBERTS, P. H. 1968 On the thermal instability of a rotating fluid sphere containing heat sources. *Phil. Trans. R. Soc. Lond.* A **263**, 93–117.

SOWARD, A. M. 1977 On the finite amplitude thermal instability of a rapidly rotating fluid sphere. *Geophys. Astrophys. Fluid Dyn.* **9**, 19–74.

SPARROW, E. M., GOLDSTEIN, R. J. & JONSSON, V. H. 1964 Thermal instability in a horizontal fluid layer: effect of boundary conditions and nonlinear temperature profile. *J. Fluid Mech.* **18**, 513–528.